Model of optogalvanic effects in the neon positive column

D. K. Doughty and J. E. Lawler
Department of Physics, University of Wisconsin, Madison, Wisconsin 53706
(Received 4 February 1983)

An experimental and theoretical investigation of the 594.5-nm optogalvanic effect in the Ne positive column is described. The effect is a decrease in discharge conductance due to laser-induced depletion of metastable atoms. Absolute measurements of the effect per unit of absorbed laser power are reported for a wide range of discharge conditions. Postive-column discharges with radius-pressure products of 0.1—1.0 cm Torr and with sustaining direct currents of 1—16 mA are studied. The effect is modeled in this regime by applying perturbation theory to key rate equations that describe the discharge. The model predictions are in agreement with the experimental measurements. Absolute densities of atoms excited to the $2p^5 3s$ levels are also reported. The regime studied covers the transition from a discharge sustained primarily by single-step electron-impact ionization to a discharge sustained primarily by two-step ionization via the $2p^5 3s$ metastable levels. The global power balance of the discharge is dominated by wall losses of atoms excited to the $2p^5 3s$ levels at all pressures and currents studied.

I. INTRODUCTION

Optogalvanic effects are changes in the electrical properties of gas discharges caused by illumination with radiation having a wavelength corresponding to an atomic or molecular transition. Although the effects were first observed over 50 years ago,[1] the potential of the phenomena as a detection method in laser spectroscopy has been widely recognized only recently.[2] Optogalvanic effects are used as a detection method in trace-element detection,[3] in Doppler-free high-resolution spectroscopy,[4] in level-crossing experiments,[5] and in other laser-spectroscopy experiments.

Some optogalvanic effects correspond to an increase in discharge conductance; we call such effects positive. Other effects correspond to a decrease in discharge conductance; we call these effects negative. The most common type of negative optogalvanic effect is due to the depletion of metastable atoms by optical excitation to a level which radiates directly or indirectly to the ground state. Effects of this type were the first optogalvanic effects observed.[1,6,7] Metastable atoms play a key role in ion production in many discharges, thus the effects can be large even with an incoherent source of radiation.

In this paper we study a negative optogalvanic effect in the Ne positive column due to radiation of wavelength 594.5 nm. This wavelength corresponds to the Ne $1s_5$-$2p_4$ absorption. We report absolute measurements of the effect over a wide range of discharge conditions, and we describe a rate-equation model which is used to calculate the absolute magnitude of the effect. We find good agreement between our measurements and the model calculations. Optogalvanic effects in Ne discharges have been studied by several researchers,[8,9,10] and considerable progress has been made in interpreting various features of the negative effects in Ne. The goal of this investigation is a quantitative understanding of the absolute magnitude of the effect.

The absolute measurements of metastable atom densities and other discharge parameters that are necessary to model the 594.5-nm optogalvanic effect provide additional insight into the positive-column kinetics. It is recognized that two-step or multistep ionization processes involving metastable atoms are dominant at medium and high values of Rp (product of column radius and pressure).[11] It is expected that single-step electron-impact ionization is dominant at low values of Rp where the electrons are very energetic.[12] The absolute measurements of discharge parameters enable us to assess the relative importance of single-step versus two-step processes. We find that the regime studied in this investigation covers the transition from a discharge sustained primarily by single-step electron-impact ionization to a discharge sustained primarily by two-step processes involving the metastable atoms.

II. THEORY

The model of the optogalvanic effect developed in this section is an application of linear, steady-state perturbation theory to the key balance equations or steady-state rate equations that describe the positive-column discharge. This approach is successful in describing the positive optogalvanic effect at 587.6 nm in the He positive column.[13] We first describe the dominant processes in the Ne positive column, then formulate the balance equations that described the discharge, and finally apply perturbation theory to describe the optogalvanic effect.

We study a Ne positive-column discharge with a radius of 0.1 cm, pressures of 1—10 Torr, and sustaining direct currents of 1—16 mA. Ion-electron pairs in this discharge are lost primarily by diffusion to the wall; recombination in the bulk of the discharge is neglected. Ion-electron pairs are produced by single-step and multistep processes, both of which are included in the model. The most important multistep processes involve the long-lived, low-lying metastable levels of Ne. The density of these $2p^5 3s$ metastable atoms is measured to be as much as a factor of 100 larger than the electron density. The model of the discharge consists of a balance equation for metastable atoms, a balance equation for electrons, and a direct current equation.

The lowest excited levels in Ne are the $1s_5$ ($^3P_2$), $1s_4$ ($^3P_1$), $1s_3$ ($^3P_0$), and $1s_2$ ($^1P_1$) levels of the $2p^5 3s$ configuration. The $1s_5$ and $1s_3$ levels are true metastable levels, whereas the $1s_4$ is not a pure metastable $^3P_1$ level due to slight triplet-singlet mixing. Radiation from the $1s_4$ and $1s_2$ levels is strongly trapped in the discharge. For purposes of the model the $1s_5$, $1s_4$, and $1s_3$ levels are lumped together as a single mestastable level as indicated in Fig. 1. We use this simplication because (1) the decay rates of the $1s_5$ and $1s_3$ levels due to diffusion to the wall and the $1s_4$ level due to escape of trapped radiation are substantially smaller than the decay rate of the $1s_2$ level due to escape of trapped radiation and (2) the $1s_5$, $1s_4$, and $1s_3$ levels are all primarily ^3P in character and likely to be strongly coupled by electron collisions. We assume that the escape of trapped radiation is the dominant decay process for the $1s_2$ ($^1P_1$) level, which implies the level does not play an important role in multistep ionization. Consequently, we do not introduce a separate balance equation for this level.

The rate of change of the metastable density, dM/dt, is the production rate per unit volume minus the destruction rate per unit volume. We represent the derivative dM/dt with H, which is a function of the spatially averaged electron density n, the spatially averaged metastable density M, and the axial electric field in the column E. Production is balanced by loss in a steady state, hence

$$\frac{dM}{dt} = H(n,M,E)$$

$$= PnN - WM - TM^2 - SnM - \frac{S'nM}{4} = 0 \,. \qquad (1)$$

The production rate constant P represents both direct electron-impact excitation of metastables and indirect processes involving electron-impact excitation of higher levels followed by radiative decay to the metastable level. The rate constant P is a strong function of E/N, where N is the density of ground-state atoms. At low currents, wall losses of the metastables at a rate W are dominant. The rate W is a weighted average of the loss rate of $1s_5$ and $1s_3$ metastables due to diffusion, and of the loss rate of $1s_4$ "metastables" due to escape of trapped radiation. Figure 2 includes a plot of the diffusion loss rate of $1s_5$ and $1s_3$ metastables versus pressure which is calculated with the use of the diffusion coefficient measured by Phelps.[14] Figure 2 also includes a calculated loss rate of $1s_4$ metastables due to escape of trapped radiation. To determine this loss rate the theory of Holstein for radiation trapping is used.[15] Calculations using this theory are complicated by the line shape for the $1s_4$ level. In the region of 1 Torr the line shape is dominated by Doppler broadening. However, at 10 Torr a pressure-broadened line shape prevails. Since the theory yields two expressions for the trapped decay rate (one for Doppler-broadened lines and one for pressure-broadened lines), it is necessary to extrapolate between these two regions. The decay rate for the $1s_4$ level is determined by summing the Doppler-broadened trapped decay rate and the pressure-broadened trapped decay rate. The curve labeled W in Fig. 2 represents the average wall loss rate of metastables weighted according to the degeneracy of the $1s_5$, $1s_4$, and $1s_3$ levels. The much larger decay rate of the $1s_2$ ($^1P_1$) level due to escape of trapped radiation is also indicated in Fig. 2. The line shape for the $1s_2$ level in the entire pressure range is dominated by pressure broadening, thus the decay rate is calculated without complications.

The rate constant T represents collisions between pairs of metastable atoms. Such collisions are extremely likely to result in ionization because the pair of metastables contains 32 eV of electronic energy. The cross section for

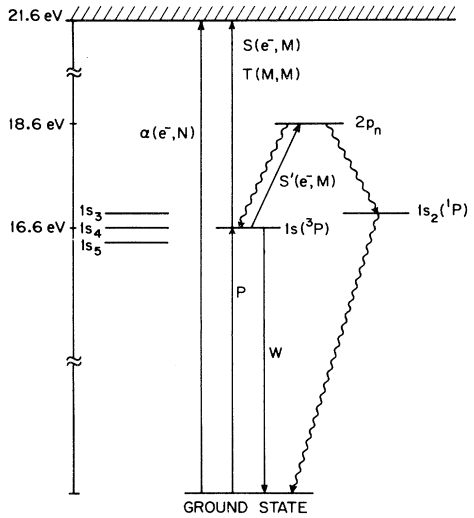

FIG. 1. Level diagrams for Ne. $1s_3$ ($^3P_2$), $1s_4$ ($^3P_1$), and $1s_5$ ($^3P_0$) levels are lumped together as a single metastable $1s$ (^3P) level. Illustrated processes are discussed in the text.

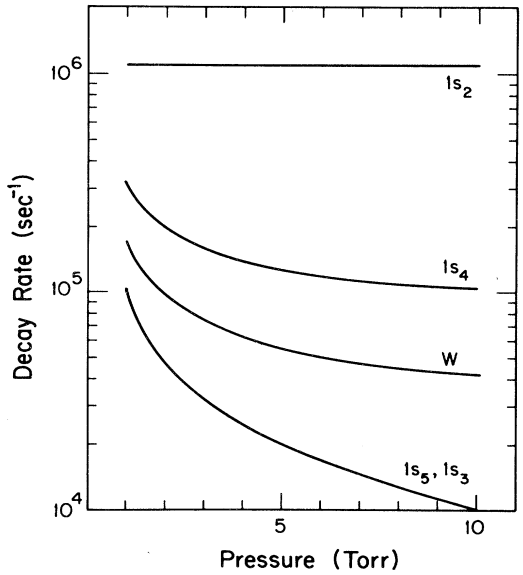

FIG. 2. Decay rates for wall processes of the four levels in the $2p^5 3s$ configuration as a function of pressure. Decay rates of the $1s_2$ and $1s_4$ levels are determined with the use of radiation trapping calculations. Decay rate of the $1s_5$ and $1s_3$ levels is determined with a measured diffusion coefficient. W is the average decay rate of the $1s_5$, $1s_4$, and $1s_3$ levels weighted according to the statistical weights of the levels.

metastable-metastable collision in Ne has been estimated, it is approximately the same as the cross section for metastable-metastable collisions in He.[16] The rate constant S represents electron-impact ionization of metastable atoms. The cross section for electron-impact ionization of $1s_5$ metastables has been measured.[17] The rate constant S is computed with the use of the measured cross section and a Maxwellian electron energy distribution at an electron temperature determined by Dote and Ichikawa.[18] We truncate the integral above 20 eV because the Maxwellian distribution overestimates the number of high-energy electrons. The energy threshold for electron-impact ionization of metastables is low (~ 5 eV), hence the rate constant S is not very sensitive to the assumed electron distribution or temperature.

The rate constant S' represents electron-impact excitation from the metastable level to the $2p_n$ levels of the $2p^5 3p$ configuration. The $2p_n$ levels decay primarily by radiation to the $1s_n$ levels ($\tau \sim 20$ nsec). An atom excited to the $2p^5 3p$ configuration has a probability of $\frac{3}{4}$ of returning to our "lumped" metastable level, and a probability of $\frac{1}{4}$ of radiating to the $1s_2$ ($^1P_1$) level and hence to the ground state. The rate constant $S'/4$ represents electron-impact destruction of metastables with no production of ions. The rate constant S' is estimated to be ten times the rate constant S.[19] This estimate is supported by the well-known cross section for excitation of Na from the $2p^6 3s$ configuration to the $2p^6 3p$ configuration.[20] Table I includes values for T, S, and S' for each pressure. The values for T, S, and S' in Table I include an enhancement factor of 1.43 to correct for the spatial distribution of electrons and metastables. The factor is the ratio of the average of the square of the lowest diffusion mode over the square of the average. All of the processes included in the metastable balance equation are indicated in Fig. 1.

The rate of change of the electron density, dn/dt, is represented with G, which is also a function of n, M, and E/N. Production of electrons is balanced by diffusion to the wall in steady state, hence

$$\frac{dn}{dt} = G(n,M,E) = \alpha v_d n + SnM + \frac{TM^2}{2} - D_a \left[\frac{2.4}{R}\right]^2 n = 0 . \quad (2)$$

Single-step ionization is represented by the product of the first Townsend coefficient α and the electron drift velocity v_d, which are strong functions of E/N. Both α and v_d are well known from drift-tube measurements,[21] but some care must be used in applying the results of drift-tube measurements to discharges with substantial fractional ($> 10^{-5}$) excitation or ionization. The two-step ionization processes involving metastables have already been introduced as a loss mechanism for metastables. The ambipolar diffusion loss rate for electrons given by $D_a(2.4/R)^2$, where D_a is the ambipolar diffusion coefficient and R is the column radius, is also tabulated in Table I.[22] Corrections to the ambipolar diffusion rate are discussed later.

The third equation necessary to model the discharge is the direct current equation

$$i = F(n,E) = env_d \pi R^2 . \quad (3)$$

The electrons in the positive column carry most of the axial current because of their larger drift velocity. Equations (1), (2), and (3) can, in principle, determine unique values of the independent variables n, M, and E if the current i is fixed by an external circuit.

The 594.5-nm optogalvanic effect studied in this work corresponds to excitation of atoms from the $1s_5$ ($^3P_2$) level to the $2p_4$ level. Atoms in the $2p_4$ level radiate with a 19-nsec lifetime to the $1s_5$, $1s_4$, and $1s_2$ levels.[23] The branching ratio β for decay to the $1s_2$ level is 0.44; it represents the probability of destroying a metastable upon absorption of a laser photon. The branching ratio is slightly less at 10 Torr due to transfer of excitation among $2p_n$ levels by neutral-atom collisions.[24]

We require that the optogalvanic effect be, at most, a 10% perturbation to i in order to apply linear perturbation theory. We further require that the optogalvanic effect be observed in the steady state. Let Q be the number of photons absorbed per unit time per unit volume. The perturbed balance equation for metastables is

$$\frac{\partial H}{\partial n}\Delta n + \frac{\partial H}{\partial M}\Delta M + \frac{\partial H}{\partial E}\Delta E = \beta Q . \quad (4)$$

The perturbed balance equation for charged particles is

$$\frac{\partial G}{\partial n}\Delta n + \frac{\partial G}{\partial M}\Delta M + \frac{\partial G}{\partial E}\Delta E = 0 . \quad (5)$$

The external circuit is a voltage source in series with a ballast resistor Z. It provides a constraint

$$Z\Delta i + l\Delta E = 0 , \quad (6)$$

where l is the length of the column. The perturbed current equation is

$$\frac{\partial F}{\partial n}\Delta n + \frac{\partial F}{\partial E}\Delta E = \Delta i = -l\Delta E/Z . \quad (7)$$

Equations (4), (5), and (7) are solved for ΔE yielding

TABLE I. Values for the metastable-metastable rate coefficient T, the electron-impact ionization rate coefficient S, the electron-impact excitation rate coefficient S', and the ambipolar diffusion loss rate $D_a(2.4/R)^2$.

Pressure (Torr)	T (10^{-9} cm^3/sec)	kTe (eV)	S (10^{-8} cm^3/sec)	S' (10^{-7} cm^3/sec)	$D_a(2.4/R)^2$ (10^6 sec^{-1})
1	2.6	4.7	6.7	6.7	9.5
2	2.6	3.9	5.4	5.4	3.9
5	2.6	2.8	2.9	2.9	1.1
10	2.6	2.2	1.6	1.6	0.44

$$\Delta E = -Q\frac{\partial F}{\partial n}\frac{\partial G}{\partial M}\left[\frac{\partial F}{\partial n}\left[\frac{\partial H}{\partial M}\frac{\partial G}{\partial E}-\frac{\partial G}{\partial M}\frac{\partial H}{\partial E}\right]+\left[\frac{\partial F}{\partial E}+\frac{l}{Z}\right]\left[\frac{\partial H}{\partial n}\frac{\partial G}{\partial M}-\frac{\partial G}{\partial n}\frac{\partial H}{\partial M}\right]\right]^{-1}. \tag{8}$$

The partial derivatives of the balance equations with respect to E are especially difficult to evaluate with the use of data from the literature. Fortunately these partials can be eliminated from Eq. (8) by introducing an empirical dynamic resistance dv/di where

$$\frac{dv}{di} = l\left[\frac{di}{dE}\right]^{-1}. \tag{9}$$

The total derivative di/dE is evaluated with the use of Eq. (3) and equations of constraint (1) and (2). Equation (8) is now simplified as

$$\Delta i = -\frac{l\Delta E}{Z} = \beta Q\frac{\partial F}{\partial n}\frac{\partial G}{\partial M} \times\left\{\left[1+Z\left[\frac{dv}{di}\right]^{-1}\right]\left[\frac{\partial H}{\partial n}\frac{\partial G}{\partial M}-\frac{\partial G}{\partial n}\frac{\partial H}{\partial M}\right]\right\}^{-1}. \tag{10}$$

The remaining partial derivatives are evaluated to yield

$$\Delta i = \beta Q i(Sn+TM) \times\left\{\left[1+Z\left[\frac{dv}{di}\right]^{-1}\right] \times\left[\left[SnM+\frac{TM^2}{2}\right]W+\left[S-\frac{S'}{4}\right]\frac{nTM^2}{2}\right]\right\}^{-1}. \tag{11}$$

Equation (11) represents the optogalvanic effect predicted by the model in a form which is convenient for comparison with measured optogalvanic effects.

III. EXPERIMENT

The experimental configuration we use to measure optogalvanic effects in the Ne positive column is indicated in Fig. 3. An actively stabilized single-frequency dye laser, tuned to the 594.5-nm transition, is mechanically chopped at 90 Hz and passed through the discharge tube. The region of the discharge tube which serves as a positive column has a length of 13.5 cm and a radius of 0.1 cm. The discharge tube has a Ne sign cathode and a tungsten pin anode which are offset from the column axis. The tube is cleaned by an extended bakeout and by repeatedly running a high-current Ne discharge followed by evacuation of the tube. Ultrahigh-purity Ne is used for all measurements. The discharge tube current is monitored across a precision 100-Ω resistor. The optogalvanic signal that appears across this resistor is measured with the use of a PAR model-124A lock-in amplifier. The ballast resistance Z is fixed at 200 kΩ. The absorbed laser power (which is proportional to Q) is measured using a calibrated thermopile.

The metastable density is measured with the use of an absorption technique. Transitions from $1s_n$ levels are optically very thick along the axis of the tube, hence we pass the laser beam across the diameter of the tube. With a path length of only 0.2 cm a relatively thick sample is still encountered as illustrated in Fig. 4. The laser power is reduced to the μW level to prevent saturation of the sample and the detector. A photodiode detects the transmitted beam as the laser is scanned across a 10-GHz frequency range. Data for the $1s_5$ ($^3P_2$), $1s_4$ ($^3P_1$), and $1s_2$ ($^1P_1$) are plotted in Figs. 5(a)–8(a). It is assumed that the $1s_3$ ($^3P_0$) density is 0.2 times the $1s_5$ density. The saturation of the $1s_5$ and $1s_4$ densities is not due to superelastic electron collisions returning atoms to the ground state, but rather to ionizing collisions as described earlier. Superelastic electron collisions are unimportant because M/N, the metastable density divided by the ground-state density, is far less than the Boltzmann factor determined from the electron temperature. The observed densities of atoms in the $1s_5$ and $1s_4$ levels support our approximation of treating these levels as a lumped metastable level. The densities of atoms in the $1s_5$ and $1s_4$ levels saturate in a similar fashion, and are roughly proportional to the statistical weight of the level. The figures indicate that at all pressures the $1s_2$ density is significantly less than the sum of the densities of the $1s_3$, $1s_4$, and $1s_5$ levels which comprise the metastable level. Furthermore, there is much less evidence of saturation of the $1s_2$ density with increasing current. These observations support the approximation that atoms in the $1s_2$ level decay primarily through the escape of resonant radiation.

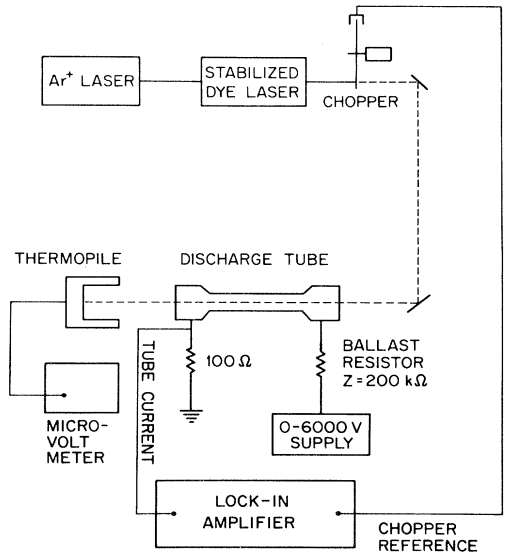

FIG. 3. Experimental configuration for measuring optogalvanic effects in the positive-column discharge.

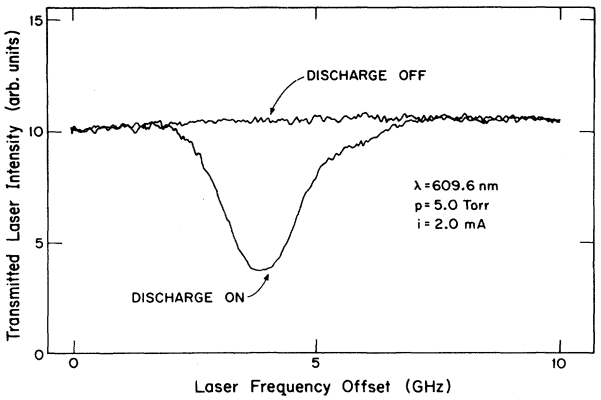

FIG. 4. Sample absorption data used to determine the densities for the $1s_5$, $1s_4$, and $1s_2$ levels.

The dynamic resistance is determined by measuring the power-supply ripple on the tube voltage and current with the use of the lock-in amplifier. Figs. 5(b)—8(b) are plots of the dynamic resistance versus current for each pressure. The large negative dynamic resistance is due to the positive-column region. The voltage drop in the cathode region is relatively independent of current. Plasma probes at the ends of the positive-column region are used to determine the voltage across the column. The voltage across the 13.5-cm-long column at 6 mA of current is 350, 345, 325, and 330 V for pressures of 1.0, 2.0, 5.0, and 10.0 Torr, respectively. The total voltage across the discharge tube is substantially larger due to the cathode fall. The electron density is determined from the measured tube current with the use of an electron drift velocity tabulated for each value of E/N.[21] The electron density as a function of current is plotted in Figs. 5(a)—8(a).

IV. COMPARISON OF EXPERIMENT AND MODEL

We characterize the strength of the optogalvanic effect with a dimensionless ratio formed by dividing the change in power delivered to the ballast resistance by the absorbed laser power. In terms of the model parameters this ratio is given by

$$P = Z 2i\Delta i / h\nu Q \pi R^2 l \,, \tag{12}$$

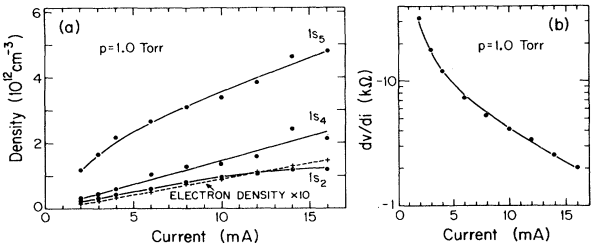

FIG. 5. (a) Plot of spatially averaged Ne excited-atom densities and the spatially averaged electron density as a function of current at 1.0 Torr. Circles indicate the measured excited-state densities for the $1s_5$, $1s_4$, and $1s_2$ levels. Crosses represent the electron density. (b) Measured dynamic resistance of the Ne discharge as a function of current at 1.0 Torr.

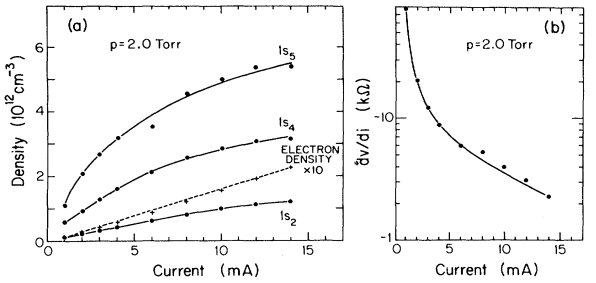

FIG. 6. (a) Measured excited-atom densities and electron density as a function of current for 2.0 Torr. (b) Dynamic resistance measurements as a function of current at 2.0 Torr.

where $h\nu$ is the energy of an absorbed photon. The expression is independent of Z for large Z, and is independent of nonessential geometrical factors such as l. Thus, we can compare optogalvanic effects in different discharges.

Experimental measurements and model calculations of the optogalvanic effect as a function of current are presented in Fig. 9 for the various pressures studied. The model calculations were performed with the use of the data in Table I, the computed values of W in Fig. 2, and empirical values for n, M, and dv/di. The model is not particularly sensitive to any one of the parameters in Table I. The model results are quite insensitive to S' except at high current and high pressure. Variations in the values of S, T, and W of at least 40% are required to produce a 20% variation in the model results. The uncertainties in the model results are between 20% and 24% due to scatter in the measured parameters M and dv/di. The uncertainties in the measured values of the optogalvanic effect are between 9% and 15%. Figure 9 indicates that the experimentally measured values of the optogalvanic effect generally agree with those calculated with the use of the model. The model begins to fail at high current and 10.0 Torr. Mechanisms, such as recombination, which have not been incorporated in the model are probably responsible for the failure of the model at high current and 10.0 Torr.

Additional insight on the importance of single-step ionization versus two-step ionization can be gained by a close

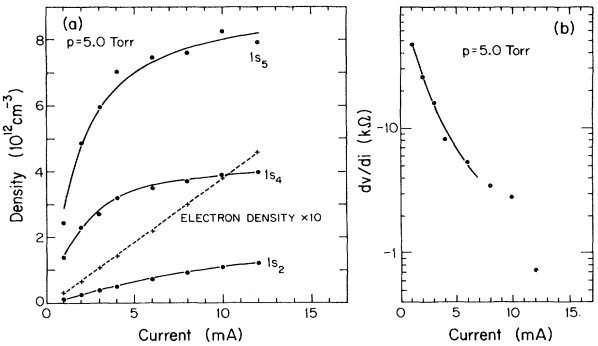

FIG. 7. (a) Measured excited-atom densities and electron density as a function of current for 5.0 Torr. (b) Dynamic resistance measurements as a function of current at 5.0 Torr.

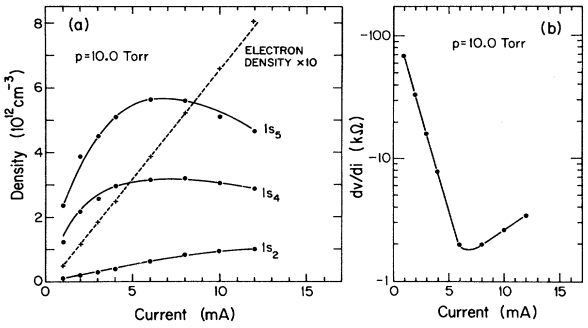

FIG. 8. (a) Measured excited-atoms densities and electron density as a function of current at 10.0 Torr. (b) Dynamic resistance measurements as a function of current at 10.0 Torr.

examination of Eq. (2). Figure 10 consists of plots of the ratio $(\alpha v_d n)/[D_a(2.4/R)^2 n]$ versus current and the ratio $(SnM+TM^2/2)/[D_a(2.4/R)^2 n]$ versus current for 1.0, 2.0, 5.0, and 10.0 Torr. The ratio of single-step ionization to total electron loss is represented by the dotted line. The ratio of two-step ionization to total electron loss is represented by the height of the cross-hatched region. If we have accurately described the dominant ionization processes, and if electron loss is accurately described by ambipolar diffusion, then the sum of the two ratios should be slightly less than 1.0. The sum of the ratios should be slightly less than 1.0 because we have not included multistep ionization processes involving a higher excited level.

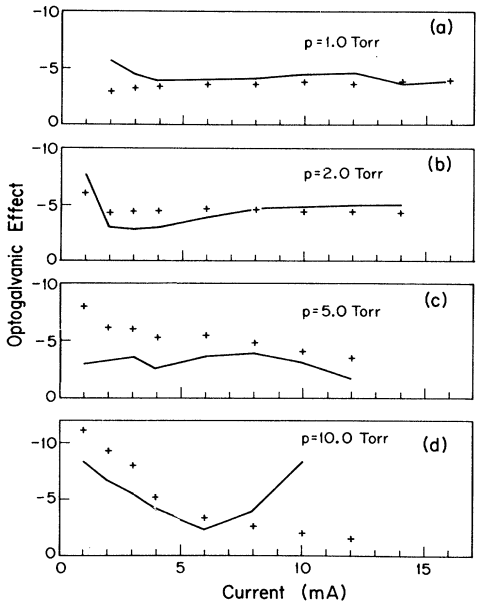

FIG. 9. 594.5-nm optogalvanic effect in Ne as a function of current for 1.0, 2.0, 5.0, and 10.0 Torr. Optogalvanic effect is the change in power delivered to the ballast resistance divided by the absorbed laser power. Solid line represents the calculated values of the optogalvanic effect using the model described in the text. Crosses indicate the measured values of the optogalvanic effect.

Such processes can be important at high current densities and high pressure.[25] Although the sum of the ratios in Fig. 10 is always close to 1.0, there are some discrepancies. The sources of the discrepancies are discussed in the following paragraphs.

The first assumption which we need examine is that Townsend coefficients from drift-tube experiments can accurately describe single-step ionization in our discharge. The electron energy distribution function in a drift tube can differ from the distribution function in a discharge at the same E/N because of electron-electron collisions and electron—excited-atom collisions. Electron-electron collisions tend to alter the distribution function so that it approaches a Maxwellian. Electron-electron collisions do not substantially alter the distribution function in this experiment because the fractional ionization does not exceed 10^{-5}. Judd investigated the effect of electron collisions with excited atoms on the electron energy distribution function in Ar.[26] Fractional excitations of 10^{-4} are reported to affect the distribution function and electron excitation rates from the ground state. The largest change in electron excitation rates occurs at low E/N near threshold for the process. Ionization rates from the ground state should behave in a fashion similar to excitation rates from the ground state because both processes sample the tail of the electron distribution function. We observe fractional excitations of 3×10^{-4} at 1.0 Torr and 16 mA current with an E/N of 7.1×10^{-16} V cm^2. Judd's calculations suggest that this fractional excitation will not alter the distribution function at such a high E/N. We observe lower fractional excitations at higher pressures. Judd's calculations indicate that we can describe single-step ionization with a Townsend coefficient. We also note that single-step ionization is not very important at 5.0 and 10.0 Torr; thus errors introduced by the use of a Townsend coeffi-

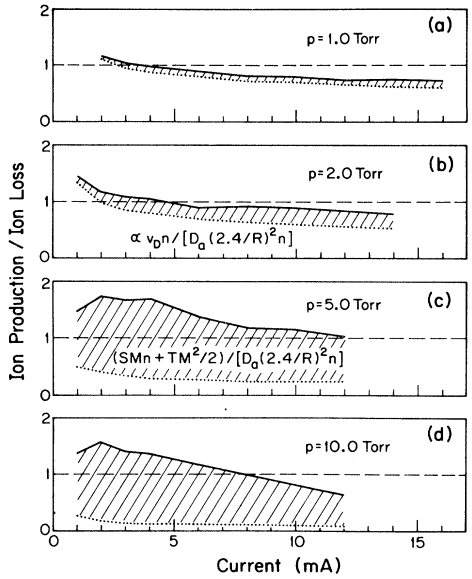

FIG. 10. Ratio of electron production to electron loss in the Ne discharge as a function of current for 1.0, 2.0, 5.0, and 10.0 Torr. Electron loss is calculated with the use of the simple expression for ambipolar diffusion.

cient are not large at 5.0 and 10.0 Torr.

The use of an ambipolar diffusion rate to describe the electron loss is not entirely satisfactory because there are two corrections to ambipolar diffusion. At low currents the expression for ambipolar diffusion underestimates the electron loss rate due to the Debye length becoming significant in comparison to the column radius. This effect, which is often described as a transition to free diffusion, has been studied theoretically by Allis and Rose,[27] among others. At low pressures the expression for ambipolar diffusion overestimates the electron loss rate due to ion inertia; the discharge is said to approach the Tonks-Langmuir free-fall regime.[28] The hydrodynamic calculations of Ingold include both effects, ion inertia and a non-negligible Debye length.[29] We use Ingold's hydrodynamic approach to calculate a correction factor f for ambipolar diffusion. Figure 11 is a plot of the data of Fig. 10 with the correction factor included. We find better agreement at 1.0 and 2.0 Torr between ion production and ion loss with the correction factor for ambipolar diffusion included. The correction factor is close to unity, even at 1.0 Torr, because the correction for ion inertia tends to cancel the correction for a nonnegligible Debye length. The latter correction is, of course, current dependent, so the cancellation is not perfect. The remaining discrepancies in Fig. 11 between ion production and ion loss are at 5.0 and 10.0 Torr. These discrepancies may be due to inaccurate values of S and T, the two-step ionization rates.

The essential point we wish to make with Figs. 10 and 11 concerns the relative importance of single-step versus two-step ionization. At 1.0 Torr single-step ionization is dominant, it is much more important than two-step ionization through the metastable level. The relative importance changes at higher pressures. Two-step ionization through the metastable level is much more important than single-step ionization at 10.0 Torr.

Further insight on the importance of the $1s_n$ levels in the discharge can be gained by an examination of the global power balance of the discharge. It is trivial to determine Ei, the total electrical input power per unit length. This power is delivered to the column wall by several mechanisms: (1) ambipolar diffusion of ion-electron pairs to the wall followed by recombination at the wall, (2) diffusion of metastable atoms to the wall followed by deexcitation at the wall, (3) leakage of trapped vacuum-ultraviolet (vuv) resonance radiation to the wall followed by absorption of the radiation in the wall, (4) emission of visible radiation followed by transmission through the wall, and (5) conduction of heat to the wall by ground-state Ne atoms. The fraction of the total input power delivered to the wall by ambipolar diffusion of ion-electron pairs is represented by the lower dotted lines of Fig. 12. The fraction of the total input power delivered to the wall by metastable $1s_5$, $1s_4$, and $1s_3$ (^3P) atoms is represented by the height of the central cross-hatched region between the dotted lines. The fraction of the total input power delivered to the wall as vuv radiation from the resonant $1s_2$ ($^1P_1$) level is represented by the height of the upper cross-hatched region. It is apparent from Fig. 12 that mechanisms (2) and (3), involving the $1s_n$ levels, are responsible for most of the power delivered to the wall at all pressures and currents studied.

The emission of visible light represents a small fraction

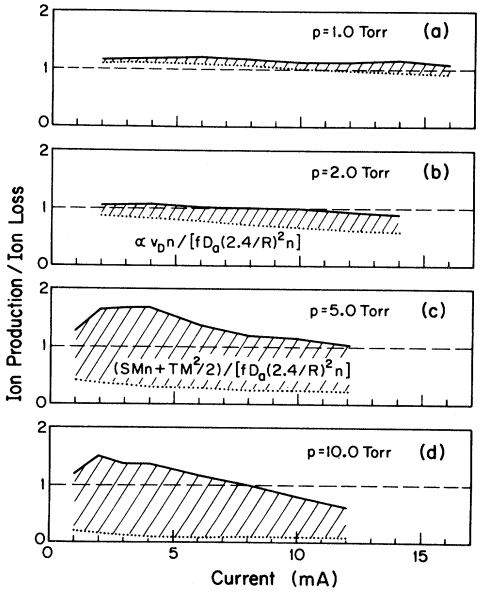

FIG. 11. Ratio of electron production to electron loss in the Ne discharge as a function of current for 1.0, 2.0, 5.0, and 10.0 Torr. Electron loss is calculated with the use of a hydrodynamic approach which includes corrections due to ion inertia and a non-negligible Debye length.

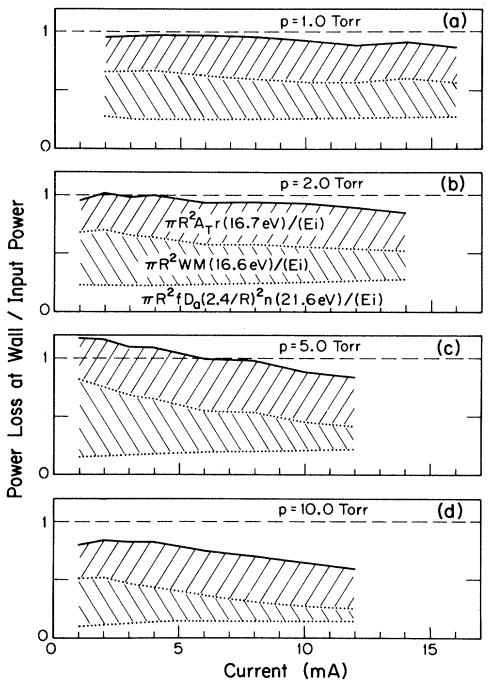

FIG. 12. Ratio of wall power output by various mechanisms to total electrical input power as a function of current for 1.0, 2.0, 5.0, and 10.0 Torr. Spatially average $1s_2$ ($^1P_1$) density r is given in Figs. 5(a)—8(a). Trapped decay rate A_T of the $1s_2$ ($^1P_1$) level is given in Fig. 2.

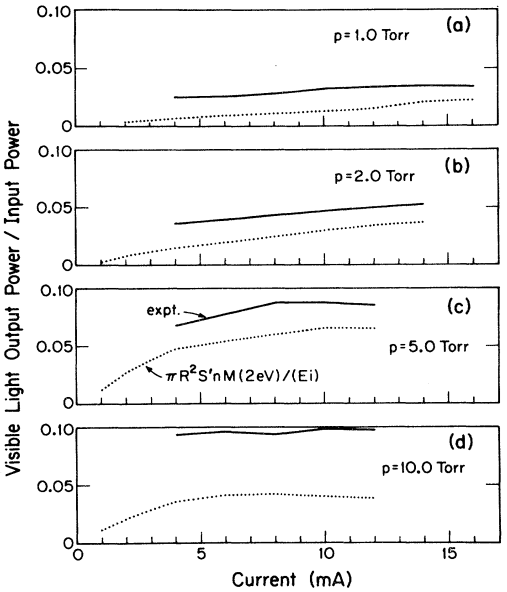

FIG. 13. Ratio of the visible-light output power to electrical input power as a function of current for 1.0, 2.0, 5.0, and 10.0 Torr. Solid lines represent measurements. Dotted lines represent our estimate of radiation due to atoms excited to the $2p^5 3p$ configuration from the metastable level.

of the input power. It is not included in Fig. 12. Most of the visible light is emitted in transitions from the $2p^5 3p$ configuration to the $2p^5 3s$ configuration. These transitions are responsible for the characteristic red color of the Ne discharge. We measure the absolute visible-light power output using a large-area silicon photodiode. The photodiode is calibrated against a Scientech thermopile with the use of a HeNe laser. The solid lines of Fig. 13 represent the visible light output power expressed as a fraction of the electrical input power. The dotted lines in Fig. 13 are plots of the ratio $\pi R^2 S' nM(2\text{ eV})/(Ei)$. It represents our estimate of radiation from atoms excited to the $2p^5 3p$ configuration from the metastable level.

V. CONCLUSION

We present a model of the negative optogalvanic effect at 594.5 nm in the Ne positive column. This model is an application of linear, steady-state perturbation theory to the key rate equations which describe the discharge. The model enables us to compute, using independently determined rate coefficients, the absolute magnitude of the optogalvanic effect in good agreement with experimental measurements. The model is tested with the use of a column radius of 0.1 cm, pressures of 1.0—10.0 Torr, and sustaining direct currents of 1—16 mA. The regime studied covers the transition from a discharge sustained primarily by single-step electron-impact ionization to a discharge sustained primarily by two-step ionization processes involving metastable atoms. Wall losses of atoms excited to the $2p^5 3s$ levels dominate the global power balance of the discharge at all pressures and currents studied.

ACKNOWLEDGMENTS

This research is supported by the U. S. Air Force Office of Scientific Research and the U. S. Army Research Office. We acknowledge helpful discussions with Dr. A. V. Phelps.

[1]F. M. Penning, Physica (Utrecht) 8, 137 (1928).
[2]R. B. Green, R. A. Keller, G. G. Luther, P. K. Schenck, and J. C. Travis, Appl. Phys. Lett. 29, 727 (1976).
[3]G. C. Turk, J. C. Travis, J. R. DeVoe, and T. C. O'Haver, Anal. Chem. 51, 1890 (1979).
[4]J. E. Lawler, A. I. Ferguson, J. E. M. Goldsmith, D. J. Jackson, and A. L. Schawlow, Phys. Rev. Lett. 42, 1046 (1979).
[5]P. Hannaford and G. W. Series, Phys. Rev. Lett. 48, 1326 (1982).
[6]C. Kenty, Phys. Rev. 80, 95 (1950).
[7]K. W. Meissner and W. F. Miller, Phys. Rev. 92, 896 (1953).
[8]K. C. Smyth and P. K. Schenck, Chem. Phys. Lett. 55, 466 (1978).
[9]K. C. Smyth, R. A. Keller, and F. F. Crim, Chem. Phys. Lett. 55, 473 (1978).
[10]E. F. Zalewski, R. A. Keller, and R. Engleman, Jr., J. Chem. Phys. 70, 1015 (1979).
[11]B. E. Cherrington, IEEE Trans. Electron Devices ED-26, 148 (1979).
[12]A. von Engel, in *Ionized Gases* (Clarendon, Oxford, 1955), p. 209.
[13]J. E. Lawler, Phys. Rev. A 22, 1025 (1980).
[14]A. V. Phelps, Phys. Rev. 114, 1011 (1959).
[15]T. Holstein, Phys. Rev. 72, 1212 (1947); 83, 1159 (1951).
[16]S. N. Salinger and J. E. Rowe, J. Appl. Phys. 39, 4299 (1968).
[17]A. J. Dixon, M. F. A. Harrison, and A. C. H. Smith, in *Abstracts of the Eighth International Conference on the Physics of Electronic and Atomic Collisions,* edited by B. C. Čobić and M. V. Kurepa (Institute of Physics, Belgrade, 1973), Vol. 1, p. 405.
[18]T. Dote and Y. Ichikawa, J. Phys. Soc. Jpn. Lett. 40, 1217 (1976).
[19]R. M. Smits and M. Prins, Physica (Utrecht) 96C, 262 (1979).
[20]J. O. Phelps and C. C. Lin, Phys. Rev. A 24, 1299 (1981).
[21]J. Dutton, J. Phys. Chem. Ref. Data 4, 577 (1975).
[22]S. C. Brown, *Basic Data of Plasma Physics* (Wiley, New York, 1959), p. 65.
[23]W. L. Wiese and G. A. Martin, in *Wavelengths and Transition Probabilities for Atoms and Atomic Ions,* Nat'l. Bur. Stand. (U.S.) Nat'l. Stand. Ref. Data. Ser. No. 68, (U.S. GPO, Washington, D.C., 1980), Pt. II, p. 386.
[24]F. C. M. Coolen, N. van Schaik, R. M. M. Smits, M. Prins, and L. W. G. Steenhuysen, Physica (Utrecht) 93C, 131 (1978).
[25]L. Vriens, J. Appl. Phys. 49, 3814 (1978).
[26]O. Judd, J. Appl. Phys. 47, 5297 (1976).
[27]W. P. Allis and D. J. Rose, Phys. Rev. 93, 84 (1954).
[28]L. Tonks and I. Langmuir, Phys. Rev. 34, 876 (1929).
[29]J. H. Ingold, Phys. Fluids 15, 75 (1972).